1977ApJ...211...77F

THE ASTROPHYSICAL JOURNAL, 211:77–90, 1977 January 1
© 1977. The American Astronomical Society. All rights reserved. Printed in U.S.A.

GAS IN GLOBULAR CLUSTERS. I. TIME-INDEPENDENT FLOW MODELS

D. J. FAULKNER* AND K. C. FREEMAN
Mount Stromlo and Siding Spring Observatory, Research School of Physical Sciences, Australian National University
Received 1975 December 8; revised 1976 June 8

ABSTRACT

A search for Hα emission in five globular clusters has yielded upper-limit ionized hydrogen masses within the core radii of $M_{H^+} < 0.1$–$0.7\ M_\odot$. This augments the findings of previous searches for ionized hydrogen (both radio and optical) that clusters are gas deficient with respect to the mass loss predictions of evolutionary theory, if the gas remains in the cluster.

Time-independent gas flow models have been constructed for globular clusters of $10^5\ M_\odot$ and $10^6\ M_\odot$, with physical assumptions chosen to maximize the predicted gas content. Ionization by electron impact was assumed, and the ionization state of both hydrogen and helium was calculated throughout the flow; the radiative cooling of the gas under these conditions was treated with considerable care. For the $10^5\ M_\odot$ cluster, steady-state flows were obtained for all gas input energies, β, down to $(2\beta)^{1/2} = 17$ km s^{-1}, and it seems certain that gas outflow will occur for all plausible stellar mass loss mechanisms. For the $10^6\ M_\odot$ cluster, radiative cooling prevented gas outflows for input energies less than $(2\beta)^{1/2} < 120$ km s^{-1}, and it appears that red-giant-branch mass loss will result in the gradual accumulation of gas.

Integrated surface brightness and flux values for the flow models showed no clear conflict with the presently observed upper limits for the 21 cm line, the radio free-free, and Hα. In the 21 cm line case, however, the observations are on the threshold of the predicted emission for $10^5\ M_\odot$ cluster flow models with no photoionization and with very low gas ejection energy, and further attempts to detect neutral hydrogen seem well worthwhile.

Subject headings: clusters: globular — hydrodynamics — interstellar: matter — radio sources: 21 cm radiation — stars: mass loss

I. INTRODUCTION

Current evolutionary theory indicates that low-mass stars evolving in globular clusters lose an appreciable proportion of their mass before reaching the white dwarf stage. The observed properties of cluster horizontal branch (HB) stars (height above the main-sequence [MS] turnoff, spread in effective temperature, and star numbers relative to the giant branch [GB]) are best explained by the hypothesis that there is a mass loss of order 25% but with some spread, between the MS and the HB (Demarque and Mengel 1972; Iben 1974). Furthermore, one globular cluster planetary nebula has been discovered (K648 in M15; O'Dell, Peimbert, and Kinman 1964) indicating that further mass loss can occur in the post-HB evolution. If, as seems likely, mass loss results from the outflow of unprocessed material at the stellar surface, and if the ejected mass were retained within the cluster between successive sweeps through the galactic plane ($\sim 3 \times 10^8$ years), sufficient hydrogen (100–1000 $M_\odot$) should accumulate for detection (Tayler and Wood 1975).

Attempts to observe both neutral and ionized hydrogen in globular clusters have, however, proved unsuccessful. Knapp, Rose, and Kerr (1973) have searched for 21 cm emission in eight clusters and derived upper mass limits of $M_{H^0} < 0.8$–$27\ M_\odot$ (based on a uniform sphere). Conklin and Kimble (1974) have similarly searched four clusters obtaining $M_{H^0} < 0.8$–$1.4\ M_\odot$. Hills and Klein (1973) have looked for free-free emission at 3.8 cm in five clusters and derived $M_{H^+} < 20$–$200\ M_\odot$ (again based on a uniform sphere). These upper limits imply either that one of the current assumptions of evolutionary theory is wrong (Knapp, Rose, and Kerr suggest that clusters may be as old as 2×10^{10} yr), or that gas is escaping from the cluster as fast as it is ejected from the stars (the explanation favored by Hills and Klein).

The search for ionized hydrogen has recently been extended into the optical domain with Fabry-Perot interferometer observations of 26 clusters by Smith, Hesser, and Shawl (1976). These authors too have interpreted their upper limit Hα fluxes as mass limits for ionized hydrogen, using a uniform distribution within the cluster core radius as model. They obtained $M_{H^+} < 0.3$–$92\ M_\odot$.

We have searched for Hα emission with high-resolution spectroscopy or five clusters (see § II). Once again no gas was detected. We have also calculated

* 1976 Visiting Fellow, Joint Institute for Laboratory Astrophysics of the National Bureau of Standards and University of Colorado.

© American Astronomical Society • Provided by the NASA Astrophysics Data System

1977ApJ...211...77F

TABLE 1

OBSERVED Hα SURFACE BRIGHTNESS LIMITS AND CORRESPONDING MASS LIMITS

Cluster	$S_{\mathrm{H}\alpha\,\mathrm{Obs}}$ (ergs cm^{-2} s^{-1} sr^{-1})	r_c (pc)	M_{H^+} ($M_\odot$)
NGC			
5904 M5.....	$< 1.4 \times 10^{-6}$	1.1	< 0.5
6388.....	$< 3.9 \times 10^{-6}$	0.6	< 0.16
6541.....	$< 1.5 \times 10^{-6}$	0.6	< 0.10
6864 M75.....	$< 2.7 \times 10^{-6}$	0.9	< 0.4
7089 M2.....	$< 1.1 \times 10^{-6}$	1.4	< 0.7

gas flow models to try to resolve this anomaly. Similar gas flow models have been calculated for elliptical galaxies by Burke (1968) (time-independent models) and by Mathews and Baker (1971) (time-dependent flows), and for globular clusters by Scott and Rose (1975) (time-independent). The present paper describes steady-state models with a considerably more detailed treatment of the gas physics. In all cases of uncertainty, we have adopted those assumptions which maximize the predicted gas content of the models; this gives added significance to those flow models which successfully explain the low observational limits.

II. Hα OBSERVATIONS

We have searched for Hα emission with spectra of the central regions of five clusters (see Table 1) taken with the coudé spectrograph of the 1.9 m telescope at Mount Stromlo. The integrated spectra of clusters show a strong Hα absorption line, with residual intensity in the core being 25–40% of the continuum intensity. None of these five clusters showed any apparent Hα emission superposed on this absorption profile, so our task is to put realistic limits on the Hα emission-line surface brightness for comparison with the theoretical model predictions discussed below.

The reciprocal dispersion of these spectra is 20 Å mm^{-1}, and they were taken on IIIa-J emulsion through a two-stage RCA C33063 image intensifier. Calibration wedge exposures were made on separate plates which were developed together with the cluster spectra. The slit dimensions were 20″ × 0″.7; this slit length is between one and four core radii for these clusters. For each spectrum the instrumental profile was derived from the weak comparison lines: the full width at half-intensity (FWHI) was in the range 0.9 ± 0.1 Å. Expressed as a velocity, this corresponds to a velocity dispersion of 15–20 km s^{-1}, which is significantly larger than the stellar velocity dispersion estimated for four of these clusters by Peterson and King (1975) and Illingworth (1973). (NGC 6388 with an observed velocity dispersion of 19 km s^{-1} is the only exception; see Illingworth and Freeman 1974.) We assume, therefore, that the profile width of any Hα emission line is set by the instrument profile. On the other hand, this instrumental FWHI is only about 30 percent of the typical FWHI of the cluster's Hα absorption line; i.e., we are setting limits on a narrow Hα emission line (profile width set by the instrumental profile) superposed on a relatively broad Hα absorption line.

The dominant noise source is plate grain noise. This was estimated for each spectrum from the noise in the continuum near the Hα line. Knowing this noise level and the instrumental profile, we can then derive a formal 3 σ upper limit on the equivalent width of any Hα emission. This equivalent width limit is then transformed to absolute surface brightness units (ergs cm^{-2} s^{-1} sr^{-1}) via the central surface brightnesses of the clusters in the V band (King 1966*b*; Illingworth 1973), Freeman's unpublished $V - R$ colors for these clusters, the cluster reddening (Alcaino 1973; Illingworth 1973), and the absolute calibration of the Johnson R system given in Allen (1973). These give the continuum surface brightness for the cluster spectrum (ergs cm^{-2} s^{-1} Å^{-1} sr^{-1}) near Hα. The resulting 3 σ limits on the Hα emission-line surface brightness in the cluster cores are given in Table 1. If we follow Smith, Hesser, and Shawl (1975) and assume that the H^+ is distributed uniformly in the cluster core, then the corresponding limits on M_{H^+} are between 0.1 and 0.7 $M_\odot$ (see Table 1). With this assumption, we see that the Hα searches produce *mass limits* that are at least an order of magnitude more stringent than the radio free-free observations. However, we will see in § VIII that the observational limits on *both* the Hα and the free-free central *surface brightnesses* are still much larger than the expected surface brightnesses.

III. GLOBULAR CLUSTER MODELS

The gas flows of this paper are based on two globular cluster models with total masses 10^5 $M_\odot$ and 10^6 $M_\odot$, which are typical of actual cluster masses. The cluster models were calculated after the method[1] of King (1966*a*), which relates the stellar density, ρ_*, to the radial distance from cluster center, r, through a parametric variable, W, which is essentially the negative of the gravitational potential:

$$\frac{\rho_*}{\rho_{*0}} = \frac{e^W \int_0^W e^{-\eta}\eta^{3/2}d\eta}{e^{W_0}\int_0^{W_0} e^{-\eta}\eta^{3/2}d\eta}\,; \tag{1}$$

$$\frac{d^2W}{dr^2} + \frac{2}{r}\frac{dW}{dr} = -\frac{9}{r_c^2}\frac{\rho_*}{\rho_{*0}}\,. \tag{2}$$

The subscript 0 indicates values at cluster center, and r_c (the core radius) is a scaling factor.

The cluster model is obtained by integrating outward from cluster center, where there are known boundary conditions, until the stellar density (and W)

[1] King appears to have evaluated the incomplete Γ function of eq. (1) by numerical quadrature. It may be easily expressed as a series by repeated integration by parts:

$$e^W \int_0^W e^{-\eta}\eta^{3/2}d\eta = \frac{2}{5}W^{5/2} + \frac{2}{5}\frac{2}{7}W^{7/2} + \frac{2}{5}\frac{2}{7}\frac{2}{9}W^{9/2} + \cdots. \tag{3}$$

The convergence is quite rapid for the W values of interest (1 part in 10^6 after 11, 22, 27, and 35 terms for W = 2, 7, 10, and 15, respectively).

© American Astronomical Society • Provided by the NASA Astrophysics Data System

1977ApJ...211...77F

fall to zero. This point is called the tidal radius, r_T. The subscript T is used hereafter to designate quantities at r_T.

In the King method, a cluster model is determined by the parameter W_0, which gives the central condensation or shape of the stellar density-radius relationship; r_c then determines the radius scale, and ρ_{*0} determines the density scale. All three quantities together determine the cluster mass and the mean square stellar velocity and their radial distributions. For our models we set W_0 at 7.5 and r_c at 0.5 pc. The former is typical for the clusters with which we compare our results, but the latter is at the lower end of the r_c range for those clusters. This will ensure that our models match the most tightly bound clusters, in keeping with our policy of maximizing the predicted gas content. The central densities were 1.738×10^{-18} and 1.738×10^{-17} g cm^{-3} for the $10^5\, M_\odot$ and $10^6\, M_\odot$ clusters, respectively. The value of W_0 chosen corresponds to

$$c = \log (r_T/r_c) = 1.68 \,. \tag{4}$$

Finally, the stellar mass interior to a point, M_*, was obtained by integrating the stellar density during the model calculation, and the mean square stellar velocity $\langle v^2 \rangle_*$ was obtained from the relationship

$$\langle v^2 \rangle_* = \frac{4}{3} \pi G r_c^2 \rho_{*0} \frac{1 - \frac{2}{5} W^{5/2}}{e^W \int_0^W e^{-\eta} \eta^{3/2} d\eta} \,. \tag{5}$$

IV. THE GAS FLOW EQUATIONS

We assume a spherically symmetric, time-independent gas flow in the cluster, with gas being injected into the system at a rate proportional to the local stellar density. We further assume that the gas ejected from any particular star interacts with that ejected from nearby stars and becomes thoroughly mixed over distances small compared with the scale of the overall flow; i.e., we assume that mass and energy of injected material are *locally* available to the gas system. We may then write equations for continuity of mass, momentum, and energy.

The Eulerian equation for continuity of mass is

$$\frac{1}{r^2} \frac{\partial}{\partial r} (r^2 \rho v) = \alpha \rho_* \,, \tag{6}$$

where ρ and v are the gas density and outward flow velocity, and α is the proportional rate of mass loss from stars (in s^{-1}).

The momentum and mass conservation equations lead to

$$v \frac{\partial v}{\partial r} + \frac{1}{\rho} \frac{\partial P}{\partial r} + \frac{G M_*}{r^2} = -\alpha \frac{\rho_*}{\rho} v \,, \tag{7}$$

where P is the gas pressure; we have assumed that the total mass interior to a point r is that of the stars alone, M_*, the mass of the gas itself being negligible. Since the gas is ejected isotropically *with respect to the ejecting stars*, it will contribute no momentum, but, having a mean velocity $-v$ with respect to the gas system, it will slow the system down on mixing by an amount shown on the right-hand side of equation (7).

The energy continuity equation is

$$v \frac{\partial U}{\partial r} - \frac{P v}{\rho^2} \frac{\partial \rho}{\partial r} = -R + \frac{\rho_*}{\rho} \alpha (U_\alpha + \tfrac{1}{2} v^2 - U - P/\rho) \,, \tag{8}$$

where U is the specific internal energy of the gas, and U_α is the specific energy of injection of new gas. The left-hand side alone of equation (8) represents a time-independent, adiabatic gas flow, while the terms on the right-hand side describe the energy sinks and sources causing departure from adiabaticity. The first term gives the energy loss due to radiative cooling of the gas, R being the cooling rate in ergs s^{-1} g^{-1}. The second term gives the energy input due to newly injected material. The injection energy of new gas (including the streaming energy of the stars with respect to the gas system) is $U_\alpha + \frac{1}{2} v^2$, and the excess of this over the local specific energy of the gas, U, is diminished by the work done by the injected material in expanding against the local pressure from negligible specific volume to $1/\rho$.

At any point in the cluster the injection energy of new gas will have two components: the energy of ejection of gas from the star itself, and the energy corresponding to the local mean square stellar velocity. The former may be regarded as a constant throughout the cluster, being related to the physical processes within individual stars. The latter is available from the cluster model. We may write

$$U_\alpha = \beta + \tfrac{1}{2} \langle v^2 \rangle_* \,. \tag{9}$$

The quantities α and β, the rate and energy of mass ejection from stars, may be regarded as free parameters in the system of equations (6)–(8). Values for these quantities will be discussed in § VI. In the next section we discuss physical relationships for the gas which enable us to express P, U, and R in terms of ρ and the gas temperature T. Since ρ_*, $\langle v^2 \rangle_*$, and M_* are given by the cluster model calculations, equations (6)–(8) reduce to a set of three differential equations in three dependent variables, v, ρ, and T.

Boundary conditions may be derived at cluster center either from symmetry or by expanding quantities as power series in r in equations (6) and (8). We obtain

$$\begin{aligned} v_0 &= 0 \,, \\ U_0 &= \beta + \tfrac{1}{2} \langle v^2 \rangle_{*0} - \frac{P_0}{\rho_0} - \frac{\rho_0 R_0}{\rho_{*0} \alpha} \,, \end{aligned} \quad \text{at } r = 0 \,. \tag{10}$$

No relationship between central quantities is obtained by power series expansion in equation (7), so we have one central boundary condition too few to solve equations (6)–(8) as an initial value problem. The solution of these equations is discussed further in § VI.

V. PHYSICS OF THE GAS

Since observations have been attempted for both neutral and ionized hydrogen in globular clusters, we

© American Astronomical Society • Provided by the NASA Astrophysics Data System

1977ApJ...211...77F

must exercise some care in the treatment of the gas physics. The ionization state of the gas must be calculated at each point to provide an integrated surface brightness prediction both in the 21 cm line and in the free-free continuum and Hα line. Details of the physics employed in the models are given below.

a) *Abundance*

We assume that the material ejected from the stars is unprocessed and has an abundance typical of the primordial material out of which the clusters were formed. We adopt a normal helium abundance and a heavy-element abundance of one-tenth the solar value, $(X, Y, Z) = (0.7, 0.3, 0.002)$.

b) *Ionization*

There are two possible ionization mechanisms for the gas in globular clusters: (i) photoionization by ultraviolet radiation from cluster stars, and (ii) collisional ionization by electrons. In both cases the ionization is followed by radiative recombination leading to an ionization equilibrium. Which of the two mechanisms is the more important will depend upon the cluster, and in particular upon the content of hot (largely blue HB) stars. The ionization mechanism also has implications for the energy balance of the gas system since the photoionization in process (i) constitutes a heating mechanism for the gas (a negative term in R), while the collisional ionization of process (ii) is achieved at the expense of the energy of the gas system itself. In both cases the subsequent recombination constitutes an energy sink for the system, although its importance is small compared with other radiative cooling processes.

The ionization calculations of this paper have been made using process (ii) for two reasons. The first is that, while there are undoubtedly some clusters (e.g., M3) with sufficient stellar ultraviolet to achieve process (i), the collisional process is available by default in *all* clusters. The second is that in seeking to explain the absence of gas in *all* globular clusters examined, it is desirable to adopt the conservative approach of excluding the additional photoionization energy input to the gas system which will be available to assist gas outflow in only *some* clusters. This is in keeping with our policy of maximizing the predicted gas content.

Since hydrogen is the most abundant element, its ionization was handled with some care. Burbidge, Gould, and Pottasch (1963) have treated the ionization equilibrium under process (ii). We have approximated their table for $\phi(y)$ (Table A1) to give a final expression for the fractions of ionized and neutral hydrogen:

$$\frac{f_{\mathrm{H}^+}}{f_{\mathrm{H}^0}} = \frac{2.79T}{4.77 - 0.377 \ln T}\left(1 + \frac{T}{78900}\right)e^{-157800/T} \quad (T < 312{,}550\ \mathrm{K})$$

$$f_{\mathrm{H}^+} = 1\,, \qquad f_{\mathrm{H}^0} = 0 \quad (T > 312{,}550\ \mathrm{K})\,. \tag{11}$$

The ionization of helium must also be considered since it provides a nonnegligible contribution to the electron density, N_e, which in turn affects the hydrogen Balmer line and free-free flux predictions. Since the helium contribution to N_e becomes important only when hydrogen is virtually fully ionized, and since it is considerably smaller than the hydrogen contribution (for $Y = 0.3$), we may use an approximation which describes both the first and second ionizations of helium rather than consider them separately. We write

$$(N_e)_{\mathrm{He}} = \frac{Y\rho}{2m_{\mathrm{H}}}\frac{1}{1 + \exp(43.5 - 4\ln T)} \quad (T > 20{,}000\ \mathrm{K})$$

$$= 0 \quad (T < 20{,}000\ \mathrm{K})\,. \tag{12}$$

The contribution of heavier elements to the electron density may be neglected.

c) *Gas Pressure and Specific Internal Energy*

We have assumed that the electrons and ions obey the perfect gas laws so that the pressure and specific internal energy of the gas are related to the temperature and the number density of ions and electrons in the usual way. Since we have considered the ionization of hydrogen and helium, however, this thermal component of the internal energy should be adjusted to include the energy of ionization for these two elements. We have adopted the convention that (1) for a completely neutral gas the internal energy equals the thermal energy of all particles, and (2) when there is any ionization, this is increased by 13.595 eV for every free hydrogen electron and by 78.984 eV for every pair of free helium electrons.

d) *Radiative Cooling Rate for the Gas*

The cooling rates for a plasma of solar abundance under conditions of collisional ionization have been determined in detail by Cox and Tucker (1969) and Cox and Daltabuit (1971) (hereafter CTCD). We have obtained an analytic expression for the cooling, based largely on CTCD, which is appropriate for our selected abundances. It is convenient to use a quantity ϵ, which is the cooling rate per unit volume, per electron, and per hydrogen atom. The mass cooling rate, R, is then related to ϵ by

$$R = \frac{\epsilon N_e N_{\mathrm{H}}}{\rho}\,. \tag{13}$$

We discuss the several cooling processes in turn.

i) *Free-free Emission*

The cooling rate for free-free emission by electrons in the field of ions of charge Z is

$$R = 1.42 \times 10^{-27}\frac{T^{1/2}}{\rho}N_e N_z Z^2 g_B\ \mathrm{ergs\,g^{-1}\,s^{-1}}\,, \tag{14}$$

where g_B is the integrated bremsstrahlung Gaunt

© American Astronomical Society • Provided by the NASA Astrophysics Data System

1977ApJ...211...77F

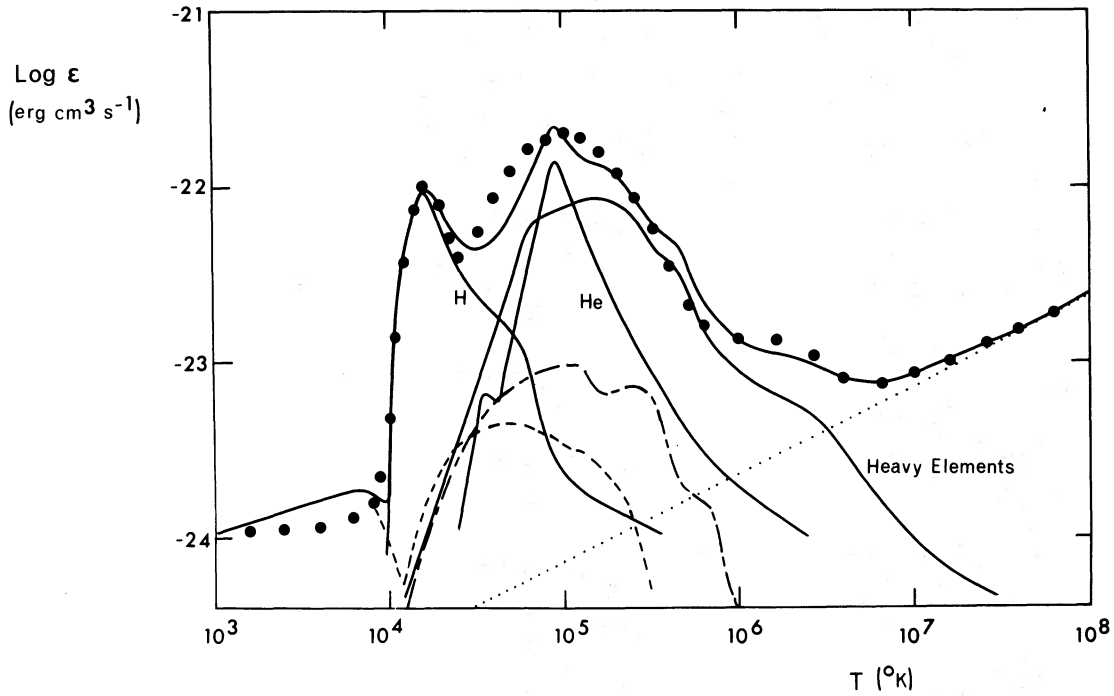

FIG. 1.—The radiative cooling coefficient for a gas with $(X, Y, Z) = (0.7, 0.3, 0.002)$ under collisional ionization conditions. The several contributions are: · · ·, free-free cooling; – – –, cooling by forbidden lines; – – – – –, by semiforbidden lines; ———, by permitted lines. The uppermost curve shows the total cooling coefficient, and the heavy dots our analytic approximation thereto (eq. [16]).

factor whose temperature dependence has been given by Karzas and Latter (1961). Free-free cooling is important relative to other mechanisms only at higher temperatures when hydrogen and helium are both fully ionized. For our selected abundances we may write

$$R = 2.3 \times 10^{-27} \frac{T^{1/2}}{\rho} N_e N_{\mathrm{H}} \quad \mathrm{ergs\ g^{-1}\ s^{-1}}, \qquad (15)$$

and the corresponding ϵ is shown in Figure 1.

ii) *Collisional Excitation of Permitted Lines*

CTCD have given plots of the permitted line ϵ values for solar abundances. We have used their results for hydrogen and helium directly and reduced their heavy element contribution by a factor of 10. The resulting contributions are shown in Figure 1.

iii) *Forbidden and Semiforbidden Lines*

Collisional excitation and radiative de-excitation of these lines also contributes to the cooling. Again we have scaled the results of CTCD by a factor of 10 (Fig. 1) since all these lines belong to heavy elements. The forbidden-line contribution is very density dependent since collisional and radiative de-excitations compete. We have used the lowest density results of CTCD. Fortunately, with our lower Z value, this density uncertainty makes little difference to the overall cooling for $T > 10^4$ K.

iv) *Recombination Radiation*

The energy losses due to recombination radiation are small compared with those for other mechanisms and may be neglected. A check for hydrogen indicated they are always less than 5 percent of the total cooling.

v) *Total Cooling Approximation*

The several contributions to the cooling rate are summed graphically in Figure 1. The total cooling may be approximated moderately well by

$$\begin{aligned}\epsilon = 10^{-23}\{&10 \exp[-14(\ln T - 9.7212)^2] \\ &+ 20 \exp[-(\ln T - 11.5129)^2] \\ &+ \exp[-(\ln T - 14.0387)^2]\} \\ &+ 2.3 \times 10^{-27}\sqrt{T} + 1 \times 10^{-24} \quad \mathrm{ergs\ cm^3\ s^{-1}}.\end{aligned} \qquad (16)$$

It should be noticed that Figure 1 indicates the cooling rate per electron and hydrogen atom. The corresponding cooling rate per gram has a temperature dependence which is broadly similar for $T > 10^4$ K, but has a sharp decrease below this value since the recombination of hydrogen removes the electrons from the plasma which inhibits the cooling mechanisms discussed above.

© American Astronomical Society • Provided by the NASA Astrophysics Data System

1977ApJ...211...77F

VI. GAS FLOW SOLUTIONS

The solution of equations (6)–(8) is characterized by two free parameters, α and β, the rate and energy of mass ejection from stars.

a) Choice of α

We may estimate α in a general way by considering the stellar evolution after the MS turnoff. We assume that the evolving stars in globular clusters were of 0.8 $M_\odot$ on the MS with $(X, Y) = (0.7, 0.3)$, and that they lose 0.2 $M_\odot$ of unprocessed material before arriving on the HB. At MS turnoff such stars have consumed 0.11 $M_\odot$ of their initial hydrogen, and in their subsequent evolution virtually the whole 0.6 $M_\odot$ of nonejected material is processed through hydrogen and helium burning. The corresponding energy release after MS turnoff is 4.8×10^{51} ergs. Luminosity functions for globular clusters (e.g., Hartwick 1970) indicate that $\sim 70\%$ of cluster light originates from post-MS stars. We may thus relate the mass loss rate to the total cluster luminosity, L, by

$$\dot{M} = 1.1 \times 10^{-19} L/L_\odot \quad (M_\odot\, \mathrm{s}^{-1}) . \qquad (17)$$

If we now employ the mass to light ratio of Illingworth (1973), 1.5 $M_\odot L_\odot{}^{-1}$, we obtain

$$\alpha = \dot{M}/M = 7 \times 10^{-20} \quad (\mathrm{s}^{-1}) . \qquad (18)$$

This result reflects the 0.2 $M_\odot$ loss before the HB; any post-HB mass loss (e.g., planetary nebulae) will increase α.

Using similar arguments Hills and Klein (1973) obtained a larger value, $\alpha = 3 \times 10^{-19}\, \mathrm{s}^{-1}$, due chiefly to their use of an older mass to light ratio for M92 (0.55 $M_\odot L_\odot{}^{-1}$) which would now be regarded as being too low. Knapp, Rose, and Kerr (1973) obtained $\alpha = 4 \times 10^{-19}\, \mathrm{s}^{-1}$ from the standard luminosity function and the observed mass loss rate for galactic stars (Pottasch 1970). Tayler and Wood (1975) used the observed numbers of HB stars in eight clusters together with the cluster masses (derived using a mass to light ratio of 1.5 $M_\odot L_\odot{}^{-1}$) to calculate $\alpha = (4 \times 10^{-20})$–$(1 \times 10^{-19})\, \mathrm{s}^{-1}$, assuming a HB evolution time of 10^8 years and 0.2 $M_\odot$ loss prior to the HB.

In keeping with our policy of erring in the direction of maximum predicted gas content, we have selected the largest of these estimates, $4 \times 10^{-19}\, \mathrm{s}^{-1}$, for our model calculations.

b) Choice of β

Little is known about the mechanism for the postulated mass loss in globular cluster stars, or, consequently, about the energy of ejected material. One obvious possibility is for dynamical mass loss at the helium flash (Edwards 1969), but more recent calculations seem to rule this out (Demarque and Mengel 1971). The most probable mechanism is stellar wind mass loss during the GB phase. There is little direct evidence for this in Population II stars (Reimers 1975), but Heasley and Mengel (1972) have shown that a wind, plausibly scaled using the average solar wind loss rate, will produce a mass loss of the required order during the GB ascent. If this is the mechanism, we may write $(2\beta)^{1/2} \approx 20\, \mathrm{km\, s}^{-1}$. This value is also typical of the planetary-nebula mass loss process. Since there is such uncertainty, however, we treat β as a free parameter and obtain gas flow solutions for all β values leading to steady-state models.

c) Integration of Flow Equations

Equations (6)–(8) must be solved in the manner of stellar wind calculations first introduced by Parker (1958, 1960*a*, *b*) for the solar wind, but used in a number of astrophysical contexts since (e.g., Finzi and Wolf 1971). In the current context the equations have been generalized for the case where the gas source and the mass giving rise to the gravitational field are both distributed throughout the gas system itself.

Wind solutions are characterized by a sonic point (at radius r_{son}) where the flow velocity (increasing outward from the center) becomes equal to the local speed of sound. Regularity of the solution at this point provides the additional boundary condition needed (with those of eq. [10]) to completely specify the problem. Unfortunately, this also ensures that it is a boundary value rather than an initial value problem, and must be solved by iteration.

Equation (6) may be rewritten as

$$r^2 \rho v = \int_0^r \rho_* \alpha r^2 dr , \qquad (19)$$

and it will be seen that the integral on the right-hand side may be evaluated, for given cluster star model and α, independently of the gas flow variables. This is a great convenience as we can provide values for ρv at each radius once for all during the *cluster* integration, and thus eliminate v from the gas flow problem, reducing it to a set of *two* differential equations in two dependent variables. The independent variable chosen was ln r, and it was found that equal intervals of 0.005 provided satisfactory precision in the numerical integrations. The dependent variables were ln ρ and ln T.

For a given cluster model and α value, there will be a single family of solutions each characterized by a β–r_{son} pair. The general procedure was to set r_{son} and integrate inward from the sonic point, iterating on β until the central boundary conditions were satisfied. The integration was then carried outward from the sonic point (to $r = 100$ pc) to complete the gas flow model.

Finally, several integrated quantities (out to the tidal radius, $r_T = 23.9$ pc) were obtained for each model. These included the mass of gas, the total cooling rate, and the total rate of doing work against gravity and in expansion against the ambient pressure. The surface brightness at cluster center, S, and the total flux, F, were also integrated for the Hα line, the radio free-free emission, and the 21 cm line.

© American Astronomical Society • Provided by the NASA Astrophysics Data System

1977ApJ...211...77F

The Hα central surface brightness may be written (Menzel 1937; Seaton 1960; Spitzer 1968, p. 15):

$$S_{\mathrm{H}\alpha} = 9.34 \times 10^{-19} \int_0^{r_T} \frac{N_e N_{\mathrm{H}^+}}{T^{3/2}} \exp\left(\frac{17530}{T} - \frac{11.412}{\ln T - 6.908}\right) dr \quad \mathrm{ergs\ cm^{-2}\ s^{-1}\ sr^{-1}}, \quad (20)$$

where we have made an analytic approximation for the temperature dependence of the departure from thermodynamic equilibrium quantity

$$b_3 = 11.79 \exp\left(-\frac{11.412}{\ln T - 6.908}\right), \quad (21)$$

from the results of Pengelly (1964).

The free-free central surface brightness may be written (Spitzer 1968, p. 21; Osterbrock 1974, p. 79):

$$S_{\mathrm{ff}} = 6.00 \times 10^{-16} \nu_{\mathrm{GHz}}^{-0.1} \int_0^{r_T} \frac{1.5 \ln T - 3.003}{T^{1/2}} \times N_e(N_{\mathrm{H}^+} + N_{\mathrm{He}^+} + 3.73\, N_{\mathrm{He}^{++}}) dr \quad \mathrm{Jy\ sr^{-1}}, \quad (22)$$

where we have approximated the radiofrequency Gaunt factor (Spitzer 1962, p. 148; Osterbrock 1974, p. 79) by

$$g_{\mathrm{ff}} = 0.551(Z\nu_{\mathrm{GHz}})^{-0.1}(1.5 \ln T - 3.003). \quad (23)$$

The integrated 21 cm line central brightness temperature, $T_b(v)$, may be written (Spitzer 1968, p. 25):

$$\int T_b(v) dv = 1.10 \times 10^{-18} \int_0^{r_T} H_{\mathrm{H}^0} dr \quad \mathrm{K\ km\ s^{-1}}. \quad (24)$$

For the 21 cm line, separate integrations were also performed to provide the *velocity profile* of the brightness temperature, allowing for both the local thermal velocity distribution of the gas and the flow velocity of the gas system.

The expression for total flux has a relationship to that for surface brightness at cluster center given by

$$S = 2\int_0^{r_T} j dr, \qquad FD^2 = 4\pi \int_0^{r_T} j r^2 dr, \quad (25)$$

where j is the emission coefficient and D the distance to the cluster.

VII. GAS FLOW MODELS

Figure 2 presents the β–r_{son} relationship for the family of solutions for each cluster model. Figures 3, 4, and 5 present the runs of velocity, temperature, and density with radius for selected models in each family. Table 2 gives model information, particularly

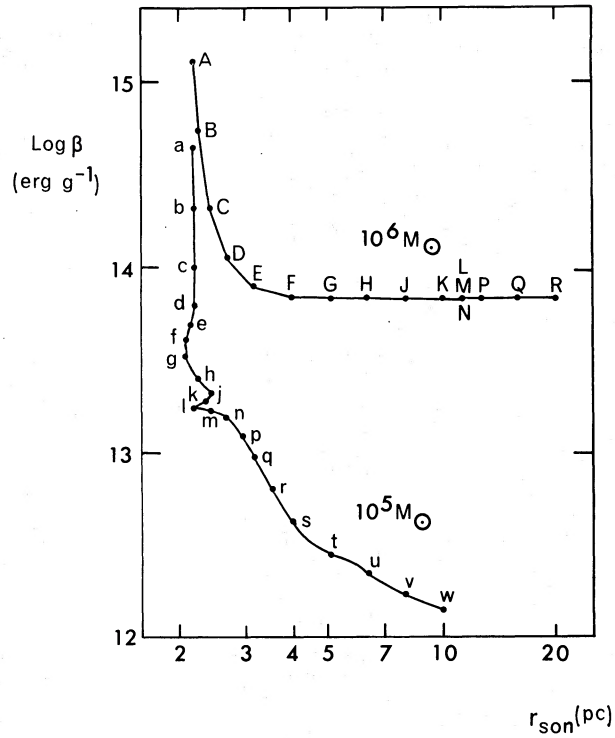

FIG. 2.—The input gas energy (β)-sonic radius (r_{son}) relationships for the two families of steady-state gas flow models for $10^5\ M_\odot$ and $10^6\ M_\odot$ globular clusters. The irregularities evident in these relationships are due to the detailed nature of our radiative cooling approximation.

the integrated properties at the tidal radius. From these it will be seen that there is a *general* relationship such that as the energy of mass loss, β, becomes smaller, the gas temperature and gas flow velocities both decrease, the sonic point moves farther from cluster center, and the gas density and mass of gas within the cluster both increase. This general relationship is somewhat complicated by the detailed form of the cooling curve we have used, which can lead (Fig. 2 and Table 2) to solutions with the same sonic radius but slightly different β values, and (in the $10^6\ M_\odot$ case) to solutions with the same β but widely different sonic radii.

There is a fundamental difference between the two flow families we have calculated, best illustrated by the f_c and f_w values of Table 2. These quantities give the fractions of incoming gas energy expended, respectively, in radiative cooling and in work against gravity and pressure. The remaining fraction of the input energy is carried out through the tidal radius by the thermal and kinetic energy of the flowing gas itself. For any cluster there will be a limiting β below which the gas has insufficient energy to overcome the gravitational potential and escape the cluster; no steady-state gas flows are possible for β less than this limit. For the $10^5\ M_\odot$ case the limit is $\beta = 1.05 \times 10^{12}$ ergs g^{-1}, and it will be seen from Figure 2 that flows were obtained for all β down to this limit. Correspondingly, in

© American Astronomical Society • Provided by the NASA Astrophysics Data System

1977ApJ...211...77F

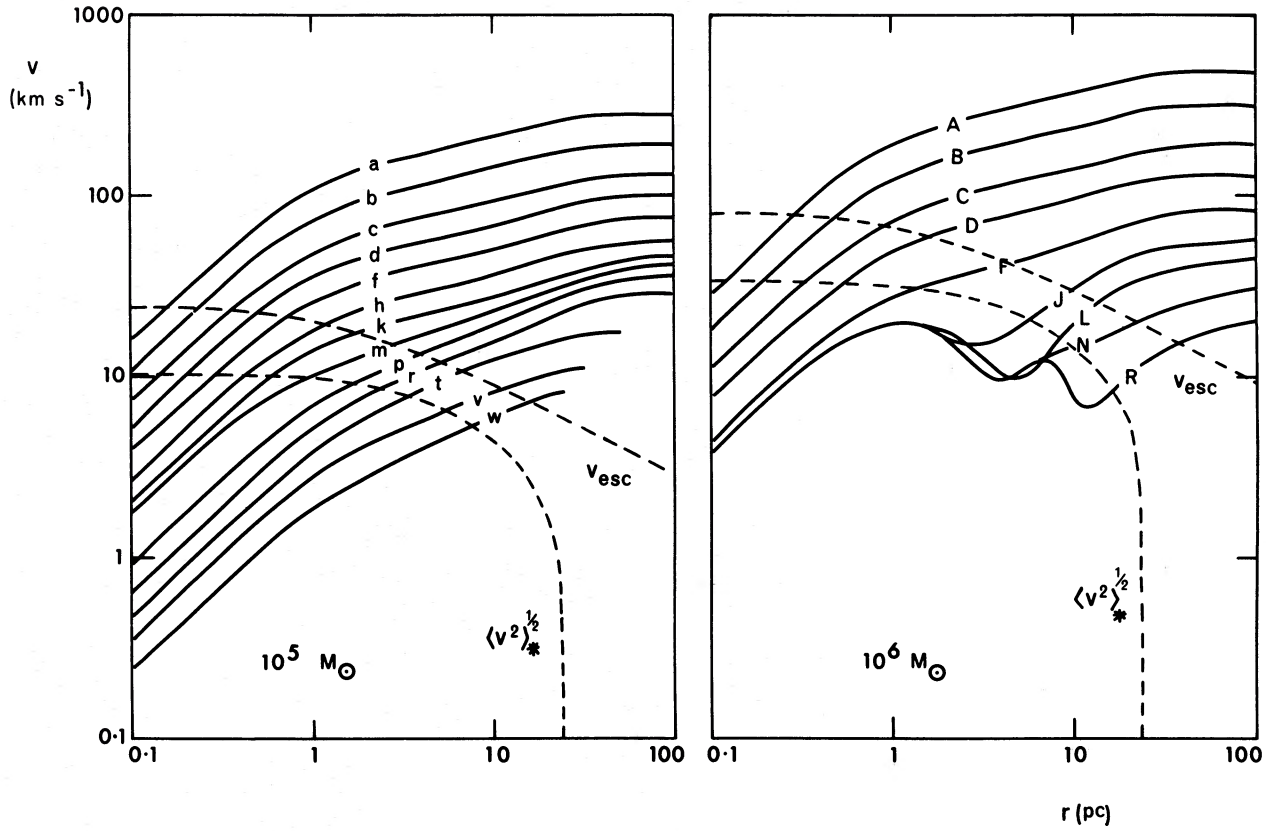

FIG. 3.—The run of velocity with radius for selected gas flow models. The curves are labeled at the sonic point. The root mean square stellar velocity and the escape velocity from the cluster are also shown.

Table 2 we see that, as β decreases, $f_w \to 1$. The corresponding limit for the 10^6 $M_\odot$ case is $\beta = 1.05 \times 10^{13}$ ergs g^{-1}, but Figure 2 indicates a flattening of the β–r_{son} relationship such that no flows were found for $\beta < 6.96 \times 10^{13}$ ergs g^{-1}. The difference is due to radiative cooling losses. For the 10^5 $M_\odot$ cluster the lower limiting β and mean stellar velocity values permit flows with low enough temperature *throughout* for radiation losses to be small (below the main bulge of the cooling curve, Figure 1). For the 10^6 $M_\odot$ cluster, however, the limiting β and mean stellar velocities are higher by a factor of 10 and the gas flows always have some part within the bulge in the cooling curve. Thus, in the lowest β flows calculated, cooling is still considerable; in fact, the cutoff is determined by $f_c \to 1$ rather than $f_w \to 1$ (Table 2).

Thus for the 10^5 $M_\odot$ cluster, steady-state flows are possible for all gas ejection energies down to $(2\beta)^{1/2} \approx 17$ km s^{-1}, and we can be reasonably confident that all plausible mechanisms for stellar mass loss will result in the outflow of gas from the cluster. For the 10^6 $M_\odot$ cluster, on the other hand, radiative cooling prevents steady-state flows for $(2\beta)^{1/2} \lesssim 118$ km s^{-1}, and only the more energetic mass loss mechanisms (e.g., MS winds) would lead to gas escape; GB winds would result in the gradual buildup of gas. Although cluster mass is the most obvious parameter determining this situation, it should be remembered that we have used cluster dimensions appropriate for the most tightly bound of actual globular clusters. Clusters more loosely bound will lose gas more readily than the models calculated here.

The important effects of radiative cooling on the gas flow characteristics are further evident in Figures 3–5. The dramatic drop in cooling rate as the gas is deprived of electrons with the recombination of hydrogen (at $\log T = 4.0$) is clearly shown by the flattening of the temperature decrease with radius as it passes through this value; this appears as a bunching of the curves in Figure 4. The complex shape of the cooling curve at the sharp H peak ($\log T = 4.2$) introduces a nonuniqueness of flow solutions when a major part of the gas system coincides with this temperature. This is seen in the complex nature of the curves for models J–R when they span this temperature range (Figures 3–5).

The mass of gas within the tidal radius increases with decreasing β for both families of gas flows, attaining 4.1 $M_\odot$ (model w) in the 10^5 $M_\odot$ case and 27.1 $M_\odot$ (model R) in the 10^6 $M_\odot$ case. The surface brightness and flux values increase with the mass of gas, but the state of ionization determines which emis-

© American Astronomical Society • Provided by the NASA Astrophysics Data System

1977ApJ...211...77F

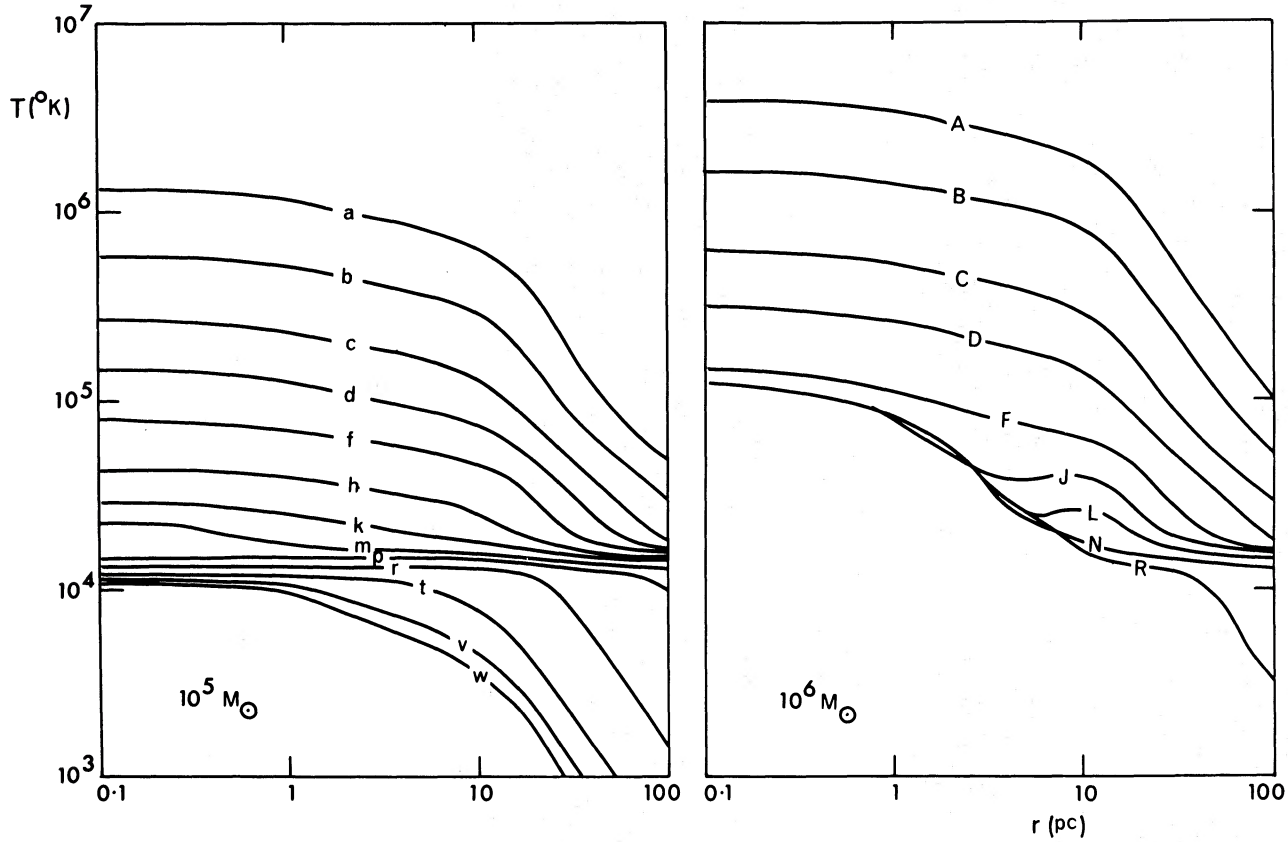

FIG. 4.—The run of temperature with radius for selected gas flow models. The curves are labeled at the sonic point.

sions are the most important. In model w the temperature is low enough throughout for virtually all the gas to be neutral, and this model has the highest 21 cm line emission of all those calculated. Model R has most of its hydrogen ionized, except in the outer parts, and this model has the highest Hα and free-free emissions calculated.

VIII. DISCUSSION

We first examine whether the predicted emissions of any of our flow models are in contradiction with the observed upper limits for 21 cm, radio free-free, and Hα. To do so, we take the flow model giving the greatest predicted emission in each case and compare the observed limits for clusters with the emission that would be observed from that flow model were it at the distances of the clusters concerned.

Figure 6 shows the velocity profile of brightness temperature at cluster center for the models with greatest 21 cm emission; we make comparisons using model w. The T_b values of Figure 6 would be appropriate for direct comparison with observed upper limits, were the telescope beamsize much smaller than the cluster dimension ($\Omega_{\rm Tel} \ll \Omega_{\rm cl}$). Integrations were also performed for the 21 cm *flux* of flow models, and these would be appropriate for comparison if $\Omega_{\rm Tel} \gg \Omega_{\rm cl}$. Unfortunately, many of the cluster observations of Knapp, Rose, and Kerr (1973) and of Conklin and Kimble (1974) are such that $\Omega_{\rm Tel} \approx \Omega_{\rm cl}$, since the linear size of the 21 cm emission is considerably larger than that of the stellar cluster with which the gas flow is associated. We performed a calculation, therefore, to interpolate predicted T_b between the central surface brightness and total flux values for model w. This was based on the approximate run of 21 cm emission with radius in the flow model and resulted in a relationship between the brightness temperature that would be observed for model w, $T_{b\,\rm w}$, and $R_{\rm obs}$, the linear radius in the model corresponding to the angular beamsize of the telescope.

The comparison with observations is given in Table 3. For each cluster the distance D (Peterson and King 1975) and telescope beam size were used to determine $R_{\rm obs}$ and hence $T_{b\,\rm w}$. The observed upper limit brightness temperature, $T_{b\,\rm obs}$, is also shown. It will be seen that no conflict arises with the observations of Knapp, Rose, and Kerr, but that the Conklin and Kimble upper limits are about two-thirds of the model w predictions. It should be remembered, however, that model w was the extreme case in our calculations, and that even the model (v) with next highest 21 cm emission would have provided no contradiction. Nevertheless, it appears that current 21 cm observations are on the threshold of the predicted emission

© American Astronomical Society • Provided by the NASA Astrophysics Data System

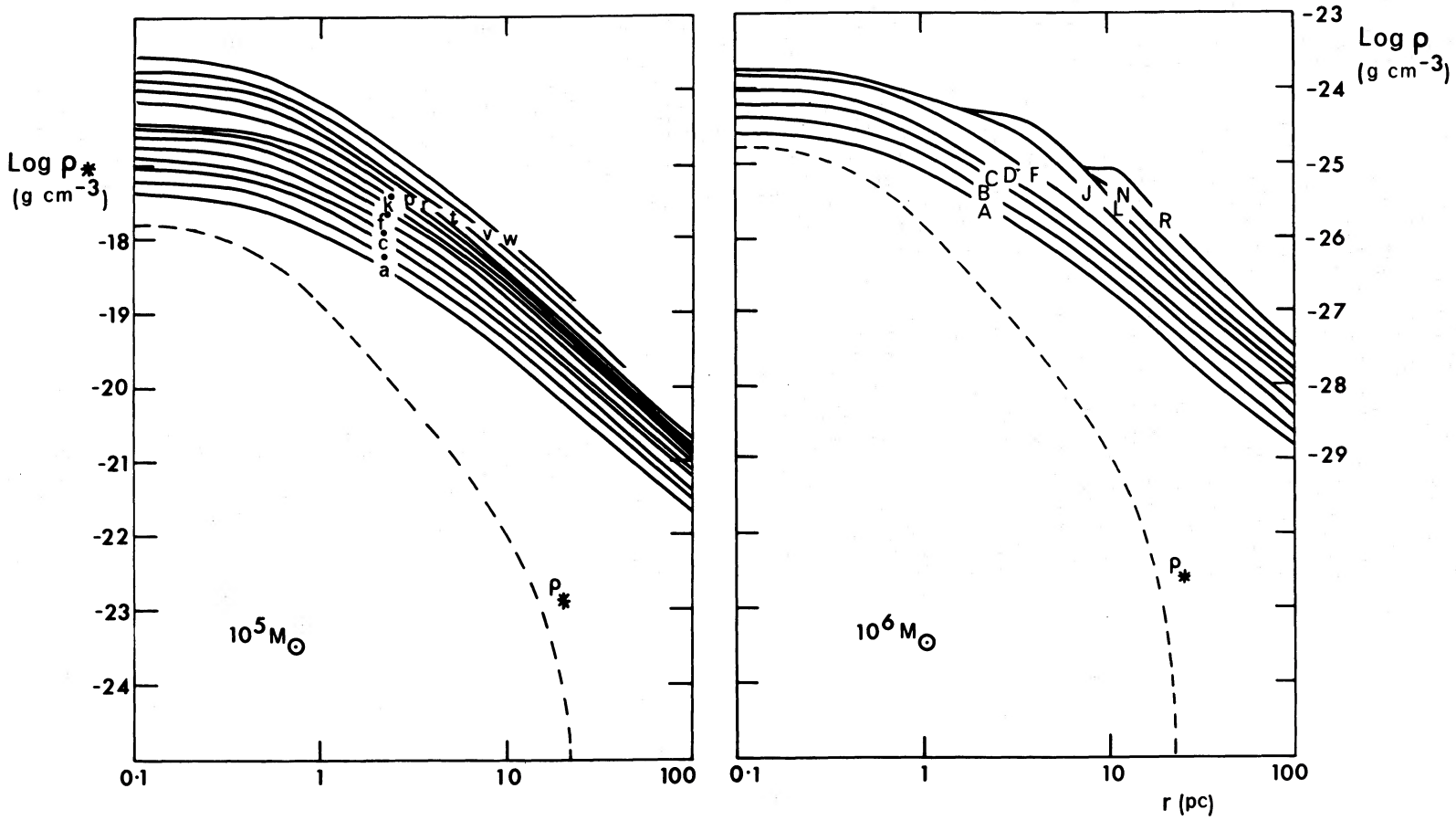

FIG. 5.—The run of density with radius for selected gas flow models. The curves are labeled at the sonic point (indicated by a dot for models B, D, H, and M). The stellar density is also indicated. Note that the scales on the left-hand and right-hand sides apply for the stellar and gas densities, respectively.

© American Astronomical Society • Provided by the NASA Astrophysics Data System

TABLE 2

SELECTED GAS FLOW MODELS

Gas Model	log r_{son} (pc)	β (erg gm^{-1})	$\sqrt{2\beta}$ (km s^{-1})	log T_o (°K)	log ρ_o (gm cm^{-3})	Properties at the Tidal Radius: v (km s^{-1})	log T (°K)	log ρ (gm cm^{-3})	M_{gas} ($M_\odot$)	Log SHA	Log SFF	T21	log t_{repl} (yr)	f_c	f_w
						10^5 $M_\odot$ Cluster									
a	0.3350	4.467(14)	299	6.11	-25.37	263	5.41	-28.35	0.11	-13.07	-2.08	-	4.96	0.00002	0.079
b	0.3375	2.100(14)	205	5.77	-25.19	176	5.06	-28.18	0.17	-12.28	-1.59	-	5.13	0.00021	0.080
c	0.3425	1.022(14)	143	5.42	-25.02	117	4.78	-28.00	0.26	-11.50	-1.10	-	5.31	0.0035	0.088
d	0.3425	6.323(13)	112	5.16	-24.88	87	4.61	-27.87	0.35	-10.93	-0.73	-	5.44	0.015	0.099
f	0.3175	4.071(13)	90	4.89	-24.74	66	4.38	-27.75	0.47	-10.35	-0.38	-	5.57	0.033	0.100
h	0.3500	2.563(13)	72	4.63	-24.58	47	4.23	-27.61	0.65	-9.81	-0.09	-	5.71	0.043	0.121
k	0.3700	1.898(13)	62	4.45	-24.47	37	4.19	-27.50	0.85	-9.40	0.16	-	5.83	0.085	0.143
m	0.3800	1.735(13)	59	4.35	-24.41	32	4.17	-27.44	1.03	-9.15	0.31	0.0014	5.91	0.208	0.144
p	0.4700	1.222(13)	49	4.16	-24.12	28	4.13	-27.37	1.25	-9.15	0.21	0.017	6.00	0.239	0.178
r	0.5500	6.528(12)	36	4.12	-23.97	23	4.02	-27.30	1.53	-9.56	-0.24	0.038	6.08	0.178	0.276
t	0.7000	2.879(12)	24	4.08	-23.82	16	3.47	-27.15	1.99	-10.29	-1.00	0.065	6.20	0.057	0.435
v	0.9000	1.741(12)	19	4.05	-23.69	11	3.23	-26.96	3.06	-10.99	-1.72	0.104	6.38	0.013	0.633
w	1.0000	1.434(12)	17	4.03	-23.53	8	3.12	-26.85	4.11	-11.35	-2.10	0.165	6.51	0.0064	0.729
						10^6 $M_\odot$ Cluster									
A	0.34	1.285(15)	507	6.58	-24.60	450	5.87	-27.59	0.67	-12.15	-0.74	-	4.72	0.00001	0.087
B	0.35	5.448(14)	330	6.20	-24.41	289	5.49	-27.39	1.04	-11.27	-0.20	-	4.92	0.00012	0.098
C	0.38	2.106(14)	205	5.78	-24.18	172	5.06	-27.17	1.75	-10.27	0.43	-	5.14	0.0022	0.128
D	0.43	1.131(14)	150	5.48	-24.01	117	4.79	-27.00	2.59	-9.57	0.89	-	5.31	0.028	0.174
F	0.60	7.090(13)	119	5.15	-23.79	71	4.53	-26.78	4.5	-8.69	1.49	-	5.55	0.222	0.220
J	0.90	6.970(13)	118	5.08	-23.73	48	4.31	-26.61	7.9	-8.29	1.74	-	5.80	0.470	0.199
L	1.05	6.967(13)	118	5.09	-23.74	34	4.23	-26.47	12.2	-8.23	1.75	-	5.99	0.584	0.192
N	1.05	6.968(13)	118	5.09	-23.74	21	4.16	-26.26	16.2	-8.21	1.75	-	6.11	0.702	0.184
R	1.30	6.968(13)	118	5.09	-23.74	12	4.10	-26.00	27.1	-8.21	1.75	0.017	6.33	0.780	0.178

SHA = central Hα surface brightness (erg cm^{-2} s^{-1} sr^{-1}).

SFF = central radio free-free surface brightness (fu sr^{-1}) x $\nu_{GHz}^{0.1}$.

T21 = central 21-cm line brightness temperature (°K) at the peak of the velocity profile (zero velocity relative to cluster centre).

t_{repl} = time for the gas within the cluster to be completely replenished by ejection from stars and outflow through the sphere through the tidal radius.

f_c = fraction of total inpu qy of gas (within the tidal radius) lost in radiative cooling.

f_w = fraction of total input energy of gas (within the tidal radius) expended in doing work against gravity and in expansion against the ambient pressure.

© American Astronomical Society • Provided by the NASA Astrophysics Data System

1977ApJ...211...77F

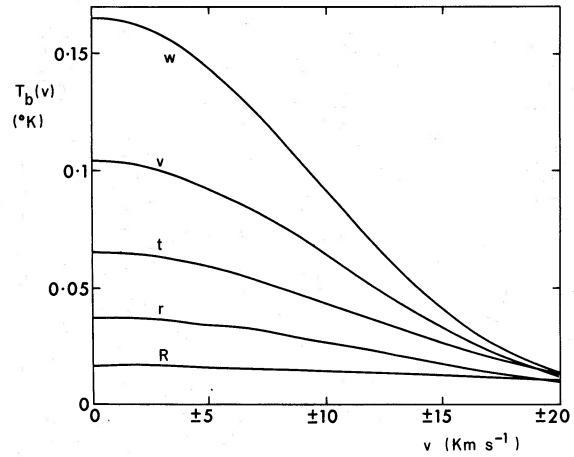

FIG. 6.—Velocity profile of the 21 cm line brightness temperature at cluster center for the gas flow models with greatest 21 cm emission.

from clusters, even when there is a steady-state gas outflow, and further attempts to detect neutral hydrogen seem well worthwhile.

The free-free observations of Hills and Klein (1973) at 3.8 cm are compared with the predictions of model R. In this case we can proceed more simply since the discrepancy between predicted and observed fluxes is so large that a very approximate comparison will suffice. We have used the central surface brightness of model R, the approximate dimensions of the free-free emission ($\sim$2 pc diameter), the Hills and Klein beam size (2′.5) and the cluster distances to derive a predicted flux from model R were it observed at the distance of each of the clusters in turn (Table 4). It will be seen that these predictions are 2000–20,000 times smaller than the Hills and Klein limits. For the Hα observations it suffices to use the central surface brightness alone since the slit covered only the central parts of the clusters we observed. The predicted brightness for model R is still appreciably smaller (200–600 times) than our observed brightness limits (Table 4). It thus appears that current observational limits for ionized hydrogen emissions are still much greater than the predictions for steady flows containing as much as 27 $M_\odot$ of gas and are unlikely to provide as critical a test on mass loss hypotheses as the neutral hydrogen observations.

We compare our results with the gas flows in globular clusters (or elliptical galaxies) obtained by Burke (1968), Mathews and Baker (1971), and Scott and Rose (1975). The present investigation has devoted greater attention to the gas physics of the problem, particularly with regard to the following: (i) *Ionization*.—All three previous investigations assumed complete photoionization of hydrogen. (ii) *Cooling rate*.—We have approximated this in some detail (it should also be noted that the direct use of CTCD rates is *not* appropriate under conditions of photoionization although this has sometimes been done). (iii) *Gas injection energy*.—The current study is the first to consider the *distribution* of mean stellar velocity in the cluster model in deriving the gas input energy at each point.

Burke (1968) obtained steady-state flows on very simplified assumptions. He used a loss rate ($\alpha = 3.2 \times 10^{-19}$ s^{-1}) comparable with ours, but confined himself to high injection energies ($[2\beta]^{1/2} \approx 300$ km s^{-1}, typical of the solar wind). This led to very high temperature (10^5–10^6 K) flows with replenishment times (10^4–10^5 years) an order of magnitude smaller than ours. Because of this Burke completely neglected radiative cooling. His results appear only marginally relevant with regard to current ideas of mass loss in globular clusters.

Scott and Rose (1975) have also computed steady-state flows for clusters. They have adopted an entirely complementary approach to ours, assuming that there is sufficient stellar ultraviolet radiation to maintain hydrogen fully ionized throughout the gas system, and that the energy input to the gas system is entirely by this photoionization; i.e., they assumed zero gas ejection energy ($U_\alpha = \beta = 0$). Their assumed mass loss rate ($\alpha = 3.2 \times 10^{-19}$ s^{-1}) was again close to ours. The Scott and Rose models are isothermal throughout, with gas temperature determined neglecting the dynamical contribution to the energy balance.

TABLE 3

COMPARISON OF PREDICTED AND OBSERVED 21 cm EMISSION

Cluster (NGC)	D (kpc)	Knapp, Rose, and Kerr (1973) (21′ beam size) R_{obs} (pc)	$T_{b\,w}$ (K)	$T_{b\,obs}$ (K)	Conklin and Kimble (1974) (5′.8 beam size) R_{obs} (pc)	$T_{b\,w}$ (K)	$T_{b\,obs}$ (K)
5272 (M3)	10.6	...	...	...	8.9	0.03	< 0.022
5904 (M5)	8.2	...	...	...	6.9	0.04	< 0.027
6121 (M4)	2.1	6.4	0.04	< 0.069			
6205 (M13)	6.3	19.2	0.01	< 0.135	5.3	0.05	< 0.033
6273 (M19)	3.0	9.2	0.03	< 0.135			
6293	6.0	18.3	0.01	< 0.240			
6341 (M92)	8.1	24.7	0.008	< 0.135			
6656 (M22)	2.9	8.9	0.03	< 0.078			
6809 (M55)	6.2	18.9	0.01	< 0.132			
7078 (M15)	10.0	30.5	0.006	< 0.120	8.4	0.03	< 0.021

© American Astronomical Society • Provided by the NASA Astrophysics Data System

1977ApJ...211...77F

TABLE 4

COMPARISON OF PREDICTED AND OBSERVED 3.8 cm FREE-FREE AND Hα EMISSIONS

Cluster (NGC)	Hills and Klein (1973) $F_{ff\,R}$ (mJy)	Hills and Klein (1973) $F_{ff\,obs}$ (mJy)	This Paper $S_{H\alpha\,R}$*	This Paper $S_{H\alpha\,obs}$*
5272 (M3)	0.001	1.9 ± 3.0		
5904 (M5)	0.002	−4.2 ± 4.6	6.2×10^{-9}	$< 1.4 \times 10^{-6}$
6205 (M13)	0.003	1.3 ± 6.2		
6341 (M92)	0.002	1.2 ± 3.5		
6388	...	...	6.2×10^{-9}	$< 3.9 \times 10^{-6}$
6541	...	...	6.2×10^{-9}	$< 1.5 \times 10^{-6}$
6864 (M75)	0.0002	0.0 ± 4.1	6.2×10^{-9}	$< 2.7 \times 10^{-6}$
7089 (M2)	...	...	6.2×10^{-9}	$< 1.1 \times 10^{-6}$

* In ergs $cm^{-2}\,s^{-1}\,sr^{-1}$.

A check with temperature decreasing linearly with radius indicated that this approximation made only a 50 percent difference to gas system properties of their models. Scott and Rose present their flow results integrated to cutoff radii which vary from 1.9 pc to 7.9 pc (chosen to match the Hills and Klein 1973 observations for particular clusters). This makes comparisons difficult, but their gas masses (0.10–36 $M_\odot$) and free-free brightness values (0.07–86 Jy sr^{-1}, apart from the NGC 6388 result) are quite comparable with ours.

Mathews and Baker (1971) have also assumed complete photoionization of hydrogen in their gas flow models for elliptical galaxies. In this case the major energy input to the system is that of supernova explosions, and they find this is sufficient to ensure steady wind-type gas outflows for most ellipticals. They used time-dependent calculations to study the buildup of such flows from zero. They also found, however, that for certain parameter choices the radiative cooling exceeded the energy input, and the gas system cooled and collapsed in the central regions. This is completely analogous to the situation that would prevail in our $10^6\,M_\odot$ case for $(2\beta)^{1/2} < 118$ km s^{-1}. Mathews and Baker modeled this collapse and argued that it resulted in the formation of $\sim 700\,M_\odot$ objects that could explain the nonthermal outbursts observed at the centers of some giant ellipticals. Time-dependent calculations to determine the fate of the gas in those *globular cluster* systems that do not have steady winds are urgently required.

Type I supernovae will occur sufficiently infrequently in a globular cluster (roughly every 3×10^7 yr, cf. flow replenishment times of 10^5–3×10^6 yr) for them to be regarded as isolated events. The effects of one explosion will have been swept from the system long before the next occurs, so there is no possibility of their providing the type of distributed energy input considered by Mathews and Baker for elliptical galaxies. The large energy associated with a Type I supernova shell ($\sim 10^{51}$ ergs; Minkowski 1968) compared with the gravitational binding energy of the gas in our flows (always $< 10^{48}$ ergs) raises the possibility that each explosion could sweep the cluster free of gas. The gas flow would then be reestablished on a time scale comparable with the replenishment time. Planetary nebulae present rather a different picture. They have ejection velocities (~ 20 km s^{-1}) quite comparable with GB stellar winds, but their frequency of occurrence in a cluster (every $\sim 3 \times 10^5$ yr) is only of the order of the replenishment time, and each event injects a mass ($\sim 0.2\,M_\odot$) which is quite a sizable fraction of the total gas mass in the flow. Thus they too should be regarded as isolated events. Their effect will be to introduce a (spatial and temporal) lumpiness into the flow system.

The gas flows we have calculated ignore any possible interaction with the galactic halo. We assume this occurs well outside the cluster tidal radius within which we have calculated our integrated gas system properties. The interaction of winds with halo material at a variety of possible densities should be investigated.

Finally, we consider the most promising approach for further observational searches for gas in globular clusters. This investigation has shown that for $10^5\,M_\odot$ clusters, GB gas ejection is likely to produce a steady-state outflow of gas, even when there is no photoionization energy input. At $10^6\,M_\odot$, on the other hand, gas buildup will occur unless the gas ejection energy is high ($\gtrsim 120$ km s^{-1}). The investigation of Scott and Rose (1975) seems to indicate that steady-state gas flows occur quite generally within clusters which have sufficient stellar ultraviolet to achieve photoionization. Furthermore, our comparison with observational limits indicates that current 21 cm studies are much closer to predicted neutral hydrogen emission rates than are the studies based on ionized hydrogen emissions. We conclude, therefore, that the most profitable line of attack is likely to be 21 cm searches of massive, tightly bound clusters with no blue HB or ultraviolet-bright stars.

REFERENCES

Alcaino, G. 1973, *Atlas of Galactic Globular Clusters* (Universidad Católica de Chile).

Allen, C. W. 1973, *Astrophysical Quantities* (3d ed.; London: Athlone Press).

© American Astronomical Society • Provided by the NASA Astrophysics Data System

1977ApJ...211...77F

Burbidge, G. R., Gould, R. J., and Pottasch, S. R. 1963, *Ap. J.*, **138**, 945.
Burke, J. A. 1968, *M.N.R.A.S.*, **130**, 241.
Conklin, E. K., and Kimble, R. A. 1974, *Bull. AAS*, **6**, 468.
Cox, D. P., and Daltabuit, E. 1971, *Ap. J.*, **167**, 113.
Cox, D. P., and Tucker, W. H. 1969, *Ap. J.*, **157**, 1157.
Demarque, P., and Mengel, J. G. 1971, *Ap. J.*, **164**, 317.
———. 1972, *Ap. J.*, **171**, 583.
Edwards, A. C. 1969, *M.N.R.A.S.*, **146**, 445.
Finzi, A., and Wolf, R. A. 1971, *Astr. Ap.*, **11**, 418.
Hartwick, F. D. A. 1970, *Ap. J.*, **161**, 845.
Heasley, J. N., Jr., and Mengel, J. G. 1972, *Observatory*, **92**, 93.
Hills, J. G., and Klein, M. J. 1973, *Ap. Letters*, **13**, 65.
Iben, I., Jr. 1974, *Ann. Rev. Astr. Ap.*, **12**, 215.
Illingworth, G. D. 1973, thesis, Australian National University.
Illingworth, G. D., and Freeman, K. C. 1974, *Ap. J.* (*Letters*), **188**, L83.
Karzas, W. J., and Latter, R. 1961, *Ap. J. Suppl.*, **6**, 167.
King, I. R. 1966*a*, *A.J.*, **71**, 64.
———. 1966*b*, *A.J.*, **71**, 276.
Knapp, G. R., Rose, W. K., and Kerr, F. J. 1973, *Ap. J.*, **186**, 831.
Mathews, W. G., and Baker, J. C. 1971, *Ap. J.*, **170**, 241.
Menzel, D. H. 1937, *Ap. J.*, **85**, 330.
Minkowski, R. 1968, in *Nebulae and Interstellar Matter*, ed. B. M. Middlehurst and L. H. Aller (Chicago: University of Chicago Press), chap. 11.
O'Dell, C. R., Peimbert, M., and Kinman, T. D. 1964, *Ap. J.*, **140**, 119.
Osterbrock, D. E. 1974, *Astrophysics of Gaseous Nebulae* (San Francisco: Freeman).
Parker, E. N. 1958, *Ap. J.*, **128**, 664.
———. 1960*a*, *Ap. J.*, **132**, 175.
———. 1960*b*, *Ap. J.*, **132**, 821.
Pengelly, R. M. 1964, *M.N.R.A.S.*, **127**, 145.
Peterson, C. J., and King, I. R. 1975, *A.J.*, **80**, 427.
Pottasch, S. R. 1970, in *IAU Symposium No. 39, Interstellar Gas Dynamics*, ed. H. J. Habing (Dordrecht: Reidel), p. 272.
Reimers, D. 1975, *Mém. Soc. Roy. Sci. Liège*, **8**, 369.
Scott, E. H., and Rose, W. K. 1975, *Ap. J.*, **197**, 147.
Seaton, M. J. 1960, *Rept. Prog. Phys.*, **23**, 313.
Smith, M. G., Hesser, J. E., and Shawl, S. J. 1976, *Ap. J.*, **206**, 66.
Spitzer, L., Jr. 1962, *Physics of Fully Ionized Gases* (New York: Interscience).
———. 1968, *Diffuse Matter in Space* (New York: Interscience).
Tayler, R. J., and Wood, P. R. 1975, *M.N.R.A.S.*, **171**, 467.

D. J. FAULKNER and K. C. FREEMAN: Mount Stromlo and Siding Spring Observatory, Canberra A.C.T., Australia

© American Astronomical Society • Provided by the NASA Astrophysics Data System